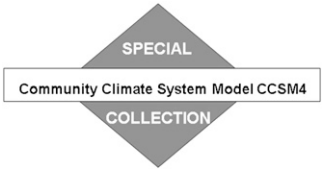

The CCSM4 Land Simulation, 1850–2005: Assessment of Surface Climate and New Capabilities

DAVID M. LAWRENCE AND KEITH W. OLESON

Earth System Laboratory, Climate and Global Dynamics Division, National Center for Atmospheric Research, Boulder, Colorado*

MARK G. FLANNER

Department of Atmospheric, Oceanic, and Space Sciences, University of Michigan, Ann Arbor, Michigan

CHRISTOPHER G. FLETCHER

Department of Physics, University of Toronto, Toronto, Ontario, Canada

PETER J. LAWRENCE, SAMUEL LEVIS, SEAN C. SWENSON, AND GORDON B. BONAN

Earth System Laboratory, Climate and Global Dynamics Division, National Center for Atmospheric Research, Boulder, Colorado*

(Manuscript received 15 February 2011, in final form 2 September 2011)

ABSTRACT

This paper reviews developments for the Community Land Model, version 4 (CLM4), examines the land surface climate simulation of the Community Climate System Model, version 4 (CCSM4) compared to CCSM3, and assesses new earth system features of CLM4 within CCSM4. CLM4 incorporates a broad set of improvements including additions of a carbon–nitrogen (CN) biogeochemical model, an urban canyon model, and transient land cover and land use change, as well as revised soil and snow submodels.

Several aspects of the surface climate simulation are improved in CCSM4. Improvements in the simulation of soil water storage, evapotranspiration, surface albedo, and permafrost that are apparent in offline CLM4 simulations are generally retained in CCSM4. The global land air temperature bias is reduced and the annual cycle is improved in many locations, especially at high latitudes. The global land precipitation bias is larger in CCSM4 because of bigger wet biases in central and southern Africa and Australia.

New earth system capabilities are assessed. The present-day air temperature within urban areas is warmer than surrounding rural areas by 1°–2°C, which is comparable to or greater than the change in climate occurring over the last 130 years. The snow albedo feedback is more realistic and the radiative forcing of snow aerosol deposition is calculated as +0.083 W m^{-2} for present day. The land carbon flux due to land use, wildfire, and net ecosystem production is a source of carbon to the atmosphere throughout most of the historical simulation. CCSM4 is increasingly suited for studies of the role of land processes in climate and climate change.

1. Introduction

Global climate models are evolving to include more earth system processes and to enhance the interactions of these processes between the component models. The Community Climate System Model, version 4 (CCSM4; Gent et al. 2011) represents a step along this path toward

* The National Center for Atmospheric Research is sponsored by the National Science Foundation.

Corresponding author address: David M. Lawrence, NCAR, P.O. Box 3000, Boulder, CO 80307-3000.
E-mail: dlawren@ucar.edu

DOI: 10.1175/JCLI-D-11-00103.1

comprehensive Earth System Models. The Community Land Model, version 4 (CLM4, Oleson et al. 2010b; Lawrence et al. 2011) is the land model that is used in CCSM4 and is a significant advance over its predecessors (Oleson et al. 2004, 2008b). New capabilities and improved parameterizations have expanded the range of studies that can be conducted with CLM and CCSM with respect to land processes and how anthropogenically or naturally evolving land states affect and interact with weather, climate, and climate change. The improvements to CLM also provide the structural foundation to incorporate additional earth system processes and to better represent existing processes in the future.

There are three main objectives for this paper. 1) We review the parameterization improvements and functional and structural advances in CLM4, which are documented in detail in Lawrence et al. (2011). 2) We document the simulation of the surface climate in CCSM4. This assessment complements previous assessments of the surface climate simulation in prior versions of CCSM (CCSM2, Bonan et al. 2002b; CCSM3, Dickinson et al. 2006). Within this analysis, we will outline the strengths and weaknesses of the model and where possible point to ways in which the model, especially the land component, can be improved in future versions of CCSM and CLM. 3) We introduce and briefly assess several new earth system features of the model. Many of these new features are examined in greater depth in separate papers in the CCSM4 Special Collection and we direct readers to the more detailed analyses where applicable.

The structure of the paper is as follows. CCSM4 and CLM4 and the simulations that are analyzed in this study are introduced in section 2. In section 3, we present an assessment of the surface climate simulation in CCSM4 with a focus on variables such as surface air temperature, precipitation, soil water storage, evapotranspiration, river discharge, and surface albedo as well as an assessment of the snow albedo feedback. In section 4, we highlight results that emphasize several new earth system capabilities in CLM4. Specifically, we examine the urban heat island derived from the CLM4 urban canyon model; the biogeophysical impact of transient land cover and land use change; the radiative forcing of aerosol deposition onto snow; terrestrial carbon fluxes and their evolution due to land use, wildfire, and net ecosystem production; the improved representation of permafrost; and the impact of prognostic vegetation state on climate variability. A discussion and summary of the strengths and weaknesses of the surface climate simulation within CCSM4 and ways in which CLM4 can be improved and expanded upon are included in section 5.

2. Description of models and simulations

a. CCSM4 and CLM4

CCSM4 is a global climate model consisting of atmosphere (R. Neale et al. 2011, unpublished manuscript), land, ocean (Danabasoglu et al. 2012), and sea ice (Holland et al. 2012) components. A general overview of CCSM4 and its performance relative to CCSM3 is provided in Gent et al. (2011). The land component of CCSM4 is CLM4 (Oleson et al. 2010b; Lawrence et al. 2011). Biogeophysical processes simulated by CLM include solar and longwave radiation interactions with vegetation canopy and soil, momentum and turbulent fluxes from canopy and soil, heat transfer in soil and snow, hydrology of canopy, soil, and snow, and stomatal physiology and photosynthesis. CLM4 contains a broad set of improvements and additions that have been provided by the CLM development community. An interim version of CLM (CLM3.5, Oleson et al. 2008b; Stöckli et al. 2008) was released in 2008. Compared to CLM3 there were changes and additions to the model hydrology, including changes to surface runoff and frozen soil parameterizations and the addition of a simple groundwater scheme. Other changes included revised canopy integration, canopy interception scaling, and a plant functional type (PFT) dependency on the soil moisture stress function. CLM3.5 exhibited a much better annual cycle of soil water storage, which was far too weak in CLM3, and an improved representation of evapotranspiration (ET), including a much more realistic partitioning of ET into its components (transpiration, soil evaporation, and canopy evaporation).

Extensive additional capabilities, input datasets, and parameterization updates have been included in CLM4. Among the most significant changes is addition of a carbon–nitrogen (CN) cycle model that is prognostic in carbon and nitrogen as well as vegetation phenology (Thornton et al. 2007; Thornton et al. 2009). A transient land cover and land use change capability, including wood harvest, has been added. The land cover change is specified for each land grid cell through annual changes in PFT area fractions, while wood harvest is specified as the annual removal of a percentage of tree PFTs (P. J. Lawrence et al. 2012). Urban climate is modeled explicitly through the inclusion of an urban canyon model (Oleson et al. 2008a). The dynamic global vegetation model (DGVM) has been expanded to include temperate and boreal shrub vegetation types (Zeng et al. 2008) and is merged with CN (CNDV) such that the carbon dynamics (e.g., productivity, decomposition, phenology, allocation, etc.) are controlled by CN while the dynamic vegetation biogeography (competition) aspects of the CLM3 DGVM (Levis et al. 2004) are retained. The biogenic volatile organic compounds emissions model is

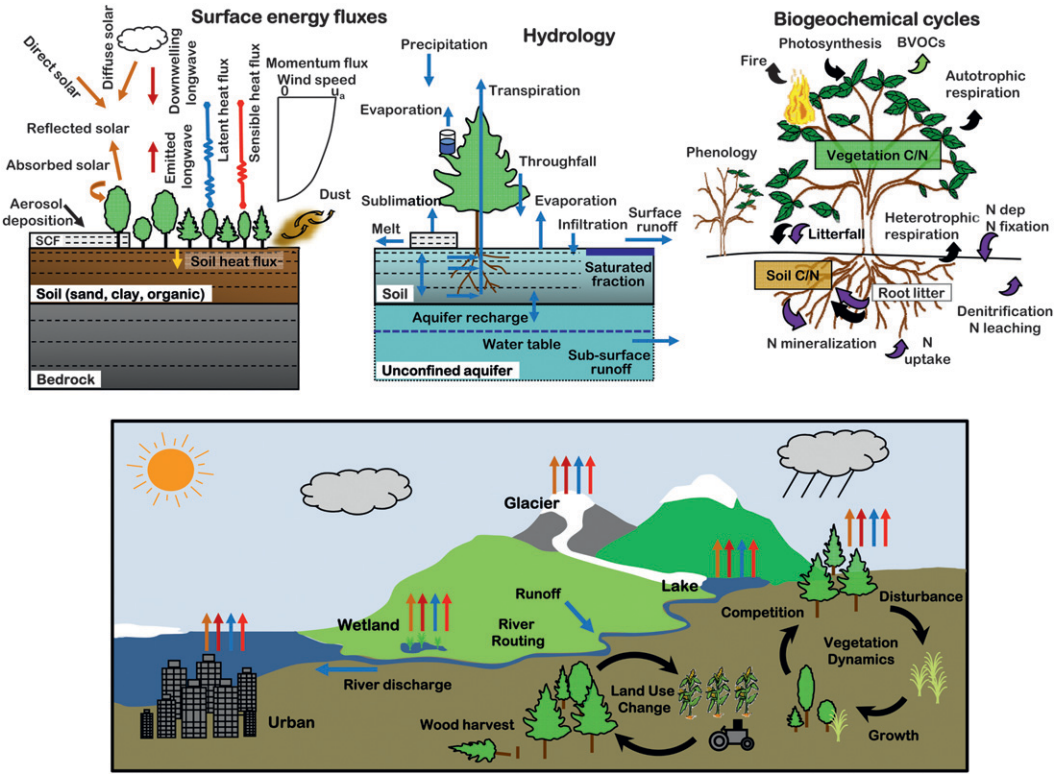

FIG. 1. Schematic representation of primary processes and functionality in the CLM4. Abbreviations are as follows: SCF; biogenic volatile organic compounds (BVOC); and carbon and nitrogen (CN). For biogeochemical cycles, black arrow denotes carbon flux, purple arrow denotes nitrogen flux. Note that not all soil levels are shown. Not all processes simulated in CLM are depicted. The flux arrows over each land type represent the solar radiation, longwave radiation, latent heat, and sensible heat fluxes that are calculated separately for each land type. Figure reproduced from Lawrence et al. (2011) with permission from the *Journal of Advances in Modeling Earth Systems*.

replaced with the Model of Emissions of Gases and Aerosols from Nature (MEGAN2) (Guenther et al. 2006; Heald et al. 2008).

The hydrology scheme has been further updated with a revised numerical solution of the Richards equation (Zeng and Decker 2009) and a modified ground evaporation parameterization that accounts for litter and within-canopy stability (Sakaguchi and Zeng 2009). The snow model incorporates the Snow and Ice Aerosol Radiation model (SNICAR; Flanner and Zender 2005, 2006; Flanner et al. 2007)—which includes aerosol deposition (black carbon and dust) onto snow, grain-size dependent snow aging, and vertically resolved snowpack heating—as well as new snow cover fraction (Niu and Yang 2007), snow burial of vegetation fraction (Wang and Zeng 2009), and snow compaction (Lawrence and Slater 2010) parameterizations. To improve the representation of permafrost, the thermal and hydrologic properties of organic soil are accounted for (Lawrence and Slater 2008) and the ground column is extended to ~50-m depth by adding 5 bedrock layers (15 total layers; Lawrence et al. 2008). The PFT distribution is as in Lawrence and Chase (2007) except with a new cropping dataset (Ramankutty et al. 2008) and with a lower grass PFT fraction in forested regions. Global energy conservation is improved by sending excess snow in snow-capped regions, which are predominantly glacier regions, into a separate ice water stream that is routed to the ocean where the energy required to melt the snow is accounted for. Effectively, this is an extremely rudimentary representation of glacier calving.

More detailed descriptions of the model improvements and the performance of CLM4 in offline mode (i.e., forced with observed meteorology) is documented in Lawrence et al. (2011) and a full documentation of the parameterizations is provided in Oleson et al. (2010b). For reference, we include a schematic diagram that depicts the main processes and functionality that exists in CLM4 (Fig. 1). To summarize, the advances relative to CLM3.5 (Oleson et al. 2008b) result in slightly higher soil moisture variability and drier average soil conditions. The new model also simulates higher snow cover, cooler soil temperatures in organic-rich soils and more extensive areas with near-surface permafrost, more global river discharge, lower albedos over forests

and grasslands, and higher transition-season albedos in snow-covered regions, all of which are improvements compared to CLM3.5. The mean biogeophysical simulation is degraded when CLM4 is run with CN because the vegetation structure is prognostic rather than prescribed. The prognostic phenology leads to a substantial increase in the interannual variability of turbulent heat fluxes.

b. Simulations

The main simulations that are analyzed here are the CCSM4 preindustrial control simulation and a five-member ensemble of historical (1850–2005) CCSM4 simulations (referred to as twentieth-century simulations). The atmosphere and land resolution is 0.9375° latitude × 1.25° longitude for these simulations. The carbon and nitrogen (CN) cycle component for the land is active, though the carbon and nitrogen fluxes are purely diagnostic and are not passed to the atmosphere and therefore do not impact atmospheric CO_2 concentrations. Even though the carbon fluxes are only diagnostic, running the model with CN active *will* have an impact on the climate simulation because the seasonal and interannual vegetation phenology [i.e., leaf area index (LAI), vegetation height] is prognostic. In the twentieth-century simulations, time varying CO_2 and other greenhouse gases and solar irradiance are prescribed. Atmospheric aerosol burden, aerosol deposition (black carbon and dust) onto snow and nitrogen deposition also vary with time, with the burdens and rates obtained from a separate twentieth-century CCSM4 run with an active chemistry component that is forced with prescribed historical emissions (Lamarque et al. 2010). Land cover changes are prescribed on an annual basis according to data from a global historical transient land use and land cover change dataset (Hurtt et al. 2006) that has been interpreted for use in CLM4 (D. M. Lawrence et al. 2012). Further details about the configuration and forcing fields for these simulations are described in Gent et al. (2011). Where applicable, the CCSM4 simulations are compared to T85 resolution CCSM3 simulations (1870 preindustrial control and a five-member ensemble of 1870–1999 historical simulations; Collins et al. (2006)). Note that vegetation phenology is prescribed and land cover is static at present-day distributions for the CCSM3 simulations. A supplementary preindustrial CCSM4 control simulation with prescribed rather than prognostic vegetation phenology (denoted CCSM4SP for "satellite phenology") is used to isolate the impact of prognostic phenology on climate variability.

Finally, several references are made throughout the paper to offline simulations in which CLM is forced with observed meteorological data (Qian et al. 2006). Two configurations of CLM4 are mentioned. The first is CLM4CN, which is the configuration with the carbon–nitrogen cycle component model active; this configuration is used in CCSM4. The second is CLM4SP where the vegetation phenology and structure is prescribed as it was in CLM3, though with updated data (Lawrence and Chase 2007). The offline CLM4 simulations are analyzed in greater detail in Lawrence et al. (2011).

3. Land surface climate simulation in CCSM3 and CCSM4

a. Surface air temperature and precipitation

The ensemble mean climatological annual cycle of surface air temperature (T_{air}) and precipitation (P) for nine representative high-latitude, midlatitude, and tropical regions for CCSM4, CCSM3, and two observational estimates for both variables are shown in Fig. 2 and Fig. 3. Based on these figures, it is difficult to draw any definitive conclusions with respect to the relative quality of the simulation in CCSM4 versus CCSM3. CCSM4 shows improvements in the annual cycle of T_{air} for Alaska and India. Over Europe the CCSM4 simulation is slightly worse. Elsewhere, the differences between the two models are difficult to distinguish or contain seasons that are better and others that are worse. Summary bias and centered root-mean-square error (RMSE) statistics for global land (excluding Antarctica) T_{air} are listed in Table 1. Based on the global land T_{air} statistics, CCSM4 is a marginally better model with a slightly smaller cold bias and about a 20% reduction in RMSE. Because of the breadth of the changes that have been implemented in all components of the coupled CCSM system, it is not possible to ascribe improvements or degradations in a variable such as T_{air} to specific changes in a particular component model.

As with temperature, inspection of the regionally averaged annual cycles of precipitation does not yield definitive conclusions about the quality of CCSM4 versus CCSM3. The CCSM3 wet bias at high latitudes remains in CCSM4, especially in the winter season. Excessive winter snowfall leads to annual maximum snow depths that are too deep (not shown but see section 4d for further discussion). Wet season precipitation in the Amazon is improved and monsoon rainfall in India is also more realistic. Globally, the mean bias is higher in CCSM4 than in CCSM3 (Table 1), due primarily to larger wet biases in central and southern Africa and Australia (not shown). The global land-centered RMSE, however, is lower by about 5% in CCSM4 (Table 1), indicating that on average there is a marginal improvement in the amplitude and phase of the precipitation annual cycle. CCSM4 also exhibits more realistic precipitation extreme event statistics over tropical land due to much stronger

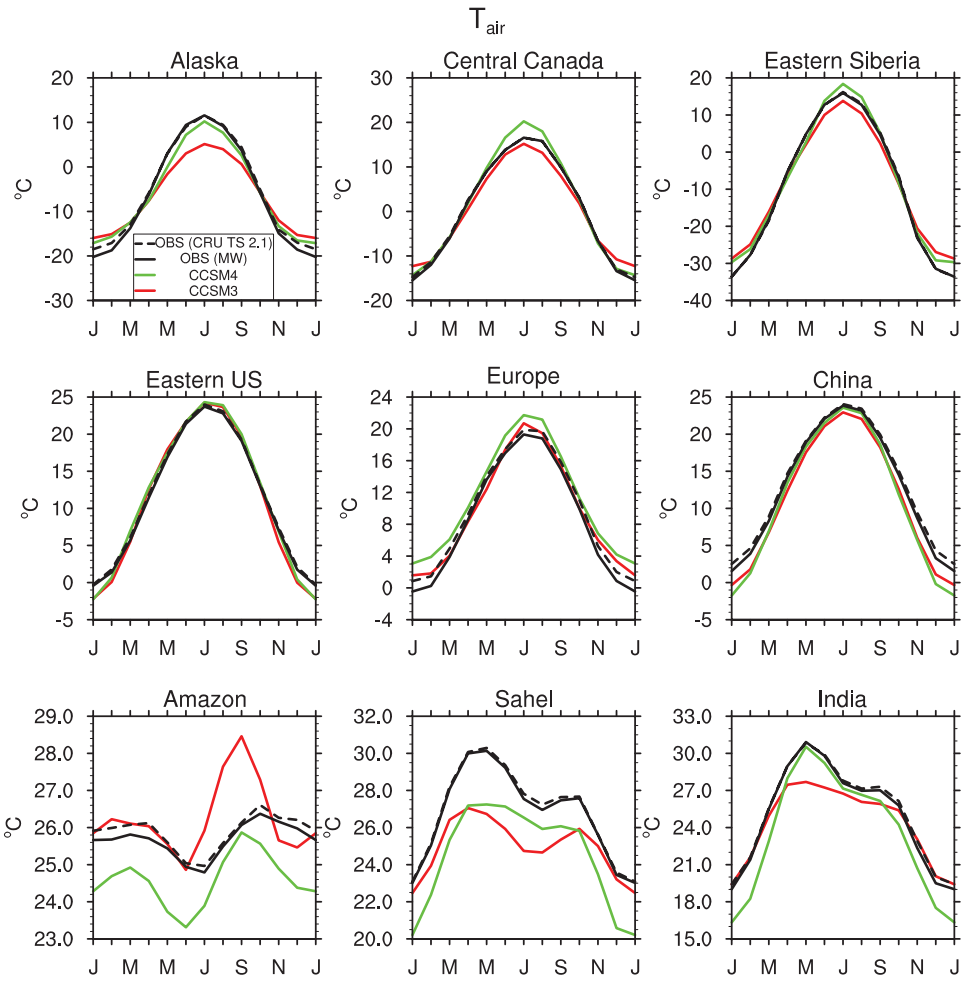

FIG. 2. Climatological annual cycle of 2-m air temperature for selected regions for CCSM4, CCSM3, and two observational estimates for the period 1980–99. The MW is the version 2.01 0.5° × 0.5° monthly time series from Matsuura and Willmott (2009b). The CRU TS 2.1 is the Climatic Research Unit 0.5° × 0.5° TS 2.1 dataset (Mitchell and Jones 2005). Regions are defined as follows: Alaska (56°–75°N, 167°–141°W), Central Canada (46°–61°N, 123°–97°W), Eastern Siberia (51°–66°N, 112°–138°E), eastern United States (27°–47°N, 92°–72°W), Europe (37°–57°N, 0°–32°E), China (18°–42°N, 100°–125°E), Amazon (14°S–5°N, 74°–53°W), Sahel (4°–19°N, 0°–32°E), and India (4°–28°N, 68°–94°E).

deep convection events that are more infrequent than the weaker events in CCSM3 (Gent et al. 2011). The improvement in precipitation statistics is related to changes in the deep convection scheme (Neale et al. 2008).

b. *Soil water storage, evapotranspiration, and runoff*

Total water storage (TWS: the sum of snow, soil moisture, groundwater, and canopy water storage) simulated by CCSM is compared to TWS observed by the Gravity Recovery and Climate Experiment (GRACE) (Tapley et al. 2004) for three representative river basins (Amazon, Mississippi, and Ob) in Fig. 4. Note that in the CCSM simulations described here, the surface water storage in rivers was not archived, but GRACE TWS estimates include surface water storage that can be a significant component of TWS in basins with large rivers such as the Amazon basin. To reduce the inconsistency in the definition of CCSM TWS and GRACE TWS, an estimate of river water storage, obtained from an offline CLM4 simulation forced with observed meteorology for the GRACE time period, is removed from the GRACE TWS.

The amplitude of the CCSM4 annual cycle of TWS for the Amazon River basin agrees well with GRACE, though the peak occurs about a month too early. By comparison, the CCSM3 annual cycle of TWS is far too weak. A weak TWS annual cycle amplitude is also seen in the Mississippi river basin in CCSM3, whereas

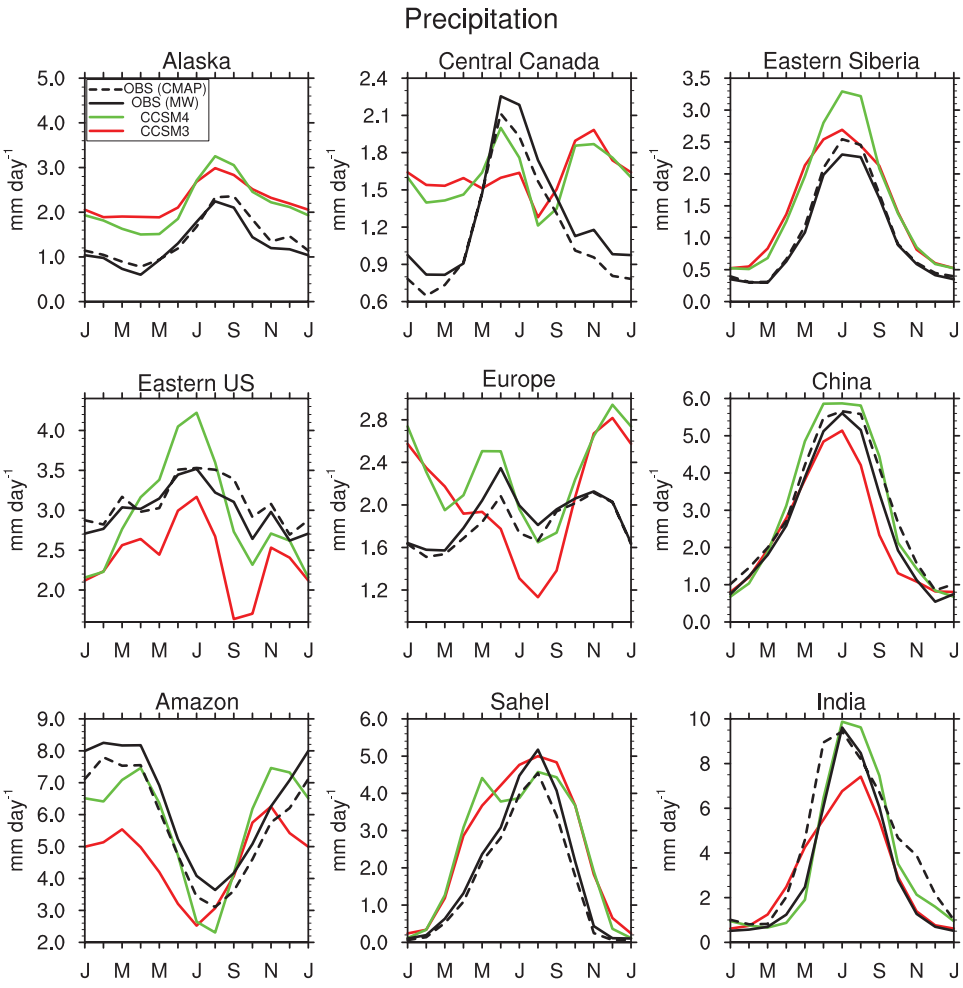

FIG. 3. As in Fig. 2, but for precipitation. CMAP is the Climate Prediction Center (CPC) Merged Analysis of Precipitation 1979–2009 "standard" (no reanalysis data) monthly time series at 2.5° × 2.5° (Xie and Arkin 1997).

in CCSM4 the TWS annual cycle agrees quite well with GRACE. In the Ob river basin, both CCSM4 and CCSM3 TWS annual cycles are larger than in GRACE, but the offline CLM4 TWS annual cycle (not shown) matches the GRACE data well, which strongly suggests that the excessive snowfall and associated snow water equivalent bias that exists in both coupled models is the source of the discrepancy in the Ob river basin. The TWS improvements seen in CCSM4 are also seen in offline CLM4 simulations (not shown) and therefore can primarily be attributed to improvements in the land model. Among the most influential sources of this improvement are reduced canopy interception, which permits more water to reach the ground, reduced runoff as a consequence of the incorporation of a simple prognostic groundwater model, improved permeability of frozen soil, and more restrictive controls on ground evaporation (Oleson et al. 2008b). The new land model has a much improved capacity to store soil water from one season to the next, which improves the simulation of latent heat flux in the dry and transition seasons. For example, the Amazon basin latent heat flux in CCSM4 remains high throughout the dry season as observed, whereas in CCSM3 the latent heat flux in the dry season drops off significantly and unrealistically (see Fig. 5).

Variability in TWS is much higher in CCSM4 in both the Amazon and Mississippi basins. In the Ob basin, the increase in interannual variability is less pronounced, probably because the interannual variability in snow water storage, which is the most variable TWS component in this region, is similar across the two models (not shown). Although the GRACE time period is short compared to the CCSM time series, comparison of the GRACE interannual variability with the CCSM variability suggests that the higher year-to-year variability in CCSM4 is more realistic.

TABLE 1. Global (excluding Antarctica for all fields) land annual mean bias and centered RMSE for the years 1980–99 for selected variables. Values in parentheses are for offline CLM4CN, CLM4SP, and CLM3. CLM4SP results are italicized. Observations are as described in Fig. 2, Fig. 3, Fig. 5, and Fig. 6. Centered RMSE is calculated from climatological annual cycle time series where the annual mean of the model data and the observation data, respectively, is removed prior to the RMSE calculation. NH SCF and NH SCA are Northern Hemisphere snow cover fraction and snow covered area (annual mean). Snow depth observed data are for North America (NA) only (1980–96) (Brown et al. 2003).

	CCSM4 annual mean bias	CCSM3 annual mean bias	CCSM4 centered RMSE	CCSM3 centered RMSE
T_{air} (°C) CRU, MW	−0.47, −0.20	−0.62, −0.35	1.30, 1.33	1.68, 1.71
P (mm day^{-1}) CMAP, MW	+0.57, +0.53	+0.24, +0.20	0.87, 0.92	0.92, 0.99
LH (W m^{-2}) FLUXNET-MTE	+13.9 (+5.8, *+2.4*)	+4.5 (+1.5)	13.2 (10.6, *9.1*)	16.6 (12.5)
River discharge (km^3 yr^{-1})	+22 (−94, *−42*)	−34 (−56)	0.96 (0.61, *0.64*)	0.83 (0.73)
NH SCF AVHRR	0.0 (−0.01, *−0.01*)	−0.04 (−0.06)	0.09 (0.08, *0.08*)	0.11 (0.10)
NH SCA, (million km^2) AVHRR (19.6)	−0.2 (−0.8, *−1.2*)	−4.3 (−5.7)		
NA snow depth (m)	+0.021 (+0.007, *+0.003*)	+0.035 (+0.011)	0.072 (0.048, *0.049*)	0.083 (0.056)

Annual cycles of latent heat flux (LH) for the same nine regions shown for T_{air} and P in Fig. 2 and Fig. 3 are shown in Fig. 5. The clearest improvement is seen in the Amazon region where the increased TWS during the rainy season prevents a large drop in LH during the dry season, though the mean LH is biased high, despite a dry bias in Amazonian precipitation. Across the tropical and midlatitude regions, LH is excessive in CCSM4, especially during the growing season. In general, the LH bias is smaller in offline CLM4CN (dashed lines in Fig. 5, Table 1) and CLM4SP (not shown) simulations, which indicates that biases in the CCSM4 climate are contributing to the CCSM4 LH bias. However, even when CLM4CN and CLM4SP is forced with observed meteorology, LH is too high (Table 1). The excessive LH in CLM4 appears to be due to several factors: a substantial high bias in LAI simulated in CLM4CN (Lawrence et al. 2011, see section 4f for further discussion), structural errors in the canopy radiative transfer, leaf photosynthesis, and stomatal conductance submodels, and model parameter errors in the photosynthetic parameter $V_{c,max}$ (Bonan et al. 2011), which together lead to excessive photosynthesis and transpiration.

In the high latitudes, LH is not as biased. LH is low in the offline CLM4CN simulation in Alaska and Eastern Siberia. This low LH bias can be traced to an apparently dry soil bias in regions with high soil organic matter contents and extensive permafrost (Lawrence et al. 2011). Preliminary investigations indicate that the dry soil bias is at least partly due to a structural error in soil water movement through icy soils. The problem is compounded in CLM4CN because the soil dry bias inhibits vegetation growth, thereby cutting off the transpiration moisture flux.

Summary statistics for LH are shown in Table 1. As implied in the regional plots in Fig. 5, the LH bias is larger in CCSM4 than CCSM3. Note that the bias in LH is also higher in CLM3 than in CLM4SP or CLM4CN (Table 1). This result does not necessarily indicate that the mean LH is more poorly simulated in CLM4 because the manner in which observed meteorological forcing is applied was modified and improved considerably between CLM3 and CLM4, which complicates direct comparisons between CLM3 and CLM4 (see Lawrence et al. 2011 for further discussion), When CLM is evaluated at flux tower sites, where the changes in the meteorological forcing method are not relevant, CLM4SP performs considerably better than CLM3 for LH and sensible heat flux for a range of time scales (Lawrence et al. 2011). In contrast to the annual mean bias, the global centered RMSE is lower in CCSM4 indicating that there has been a general improvement in the simulated phase and amplitude of the LH annual cycle. This improvement is related to significant improvements in the process level representation of ET that are included in CLM4. In CCSM3 and CLM3, the partitioning of ET was poor with very low transpiration rates leading to global ET being dominated by ground evaporation rather than transpiration (Lawrence et al. 2007; Oleson et al. 2008b). In CLM4 and CCSM4, the partitioning of ET into transpiration, ground evaporation, and canopy evaporation is much improved (Lawrence et al. 2011), which leads to more realistic land–atmosphere interactions such as, for example, a more realistic temporal response of ET to a precipitation event.

River discharge is calculated via the CLM River Transport Model (RTM, Branstetter and Famiglietti 1999), which transports gridcell runoff to the ocean via pathways that approximate the path of the real global river

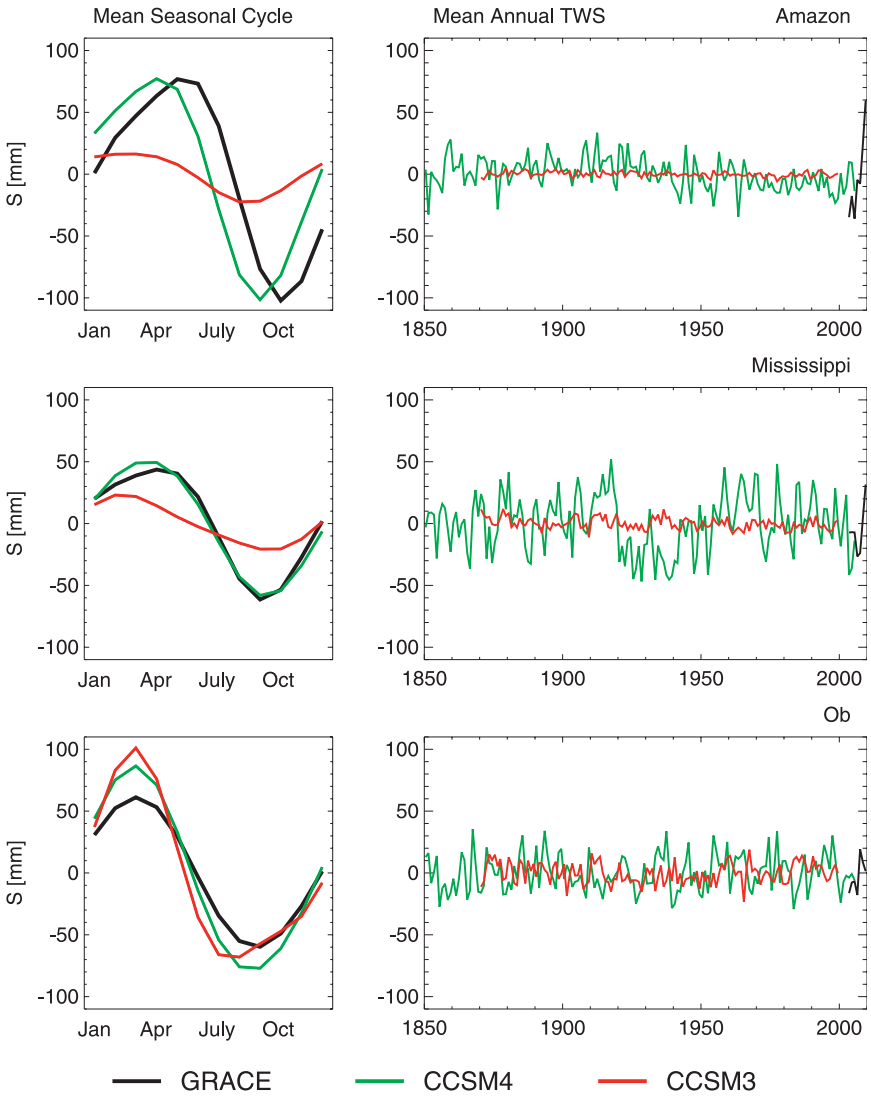

FIG. 4. Climatological (left) annual cycle and (right) monthly anomaly time series of soil water storage in CCSM3 and CCSM4 compared to estimates from GRACE for (top to bottom) the Amazon, Mississippi, and Ob River basins . CCSM3 and CCSM4 climatologies are for years 1980–99. GRACE climatology is for the period 2003–09.

network. Total discharge into the world's oceans, which is directly related to land precipitation minus evapotranspiration, is slightly degraded in CCSM4 (1.20×10^6 m^3 s^{-1} observed global discharge (Dai and Trenberth 2002); 1.30×10^6 m^3 s^{-1} in CCSM4; 1.24×10^6 m^3 s^{-1} CCSM3), probably due to the larger precipitation bias in CCSM4. However, when we consider the world's largest 50 rivers, the linear correlation coefficient of modeled versus observed river discharge is slightly improved (0.81 in CCSM4; 0.75 in CCSM3; 0.98 in CLM4CN and CLM4SP; and 0.97 in CLM3, see Fig. 6); this may be indicative of an improved spatial pattern of precipitation and evapotranspiration in CCSM4. In CCSM3, the most poorly simulated large rivers were the Amazon and Congo Rivers with far too little discharge from the Amazon River (more than 50% less discharge than observed) and far too much discharge from the Congo River (more than 100% more discharge than observed). Though the mean discharge is slightly improved for both rivers, they both remain problematic in CCSM4. For the Congo River, the bias is likely due to excessive rainfall in tropical Africa since the bias is not apparent in offline CLM4 simulations forced with observed rainfall. For the Amazon River, the low discharge bias is seen in both CCSM4 and CLM4, which implies that the bias is likely predominantly a function of excessive ET. Among the

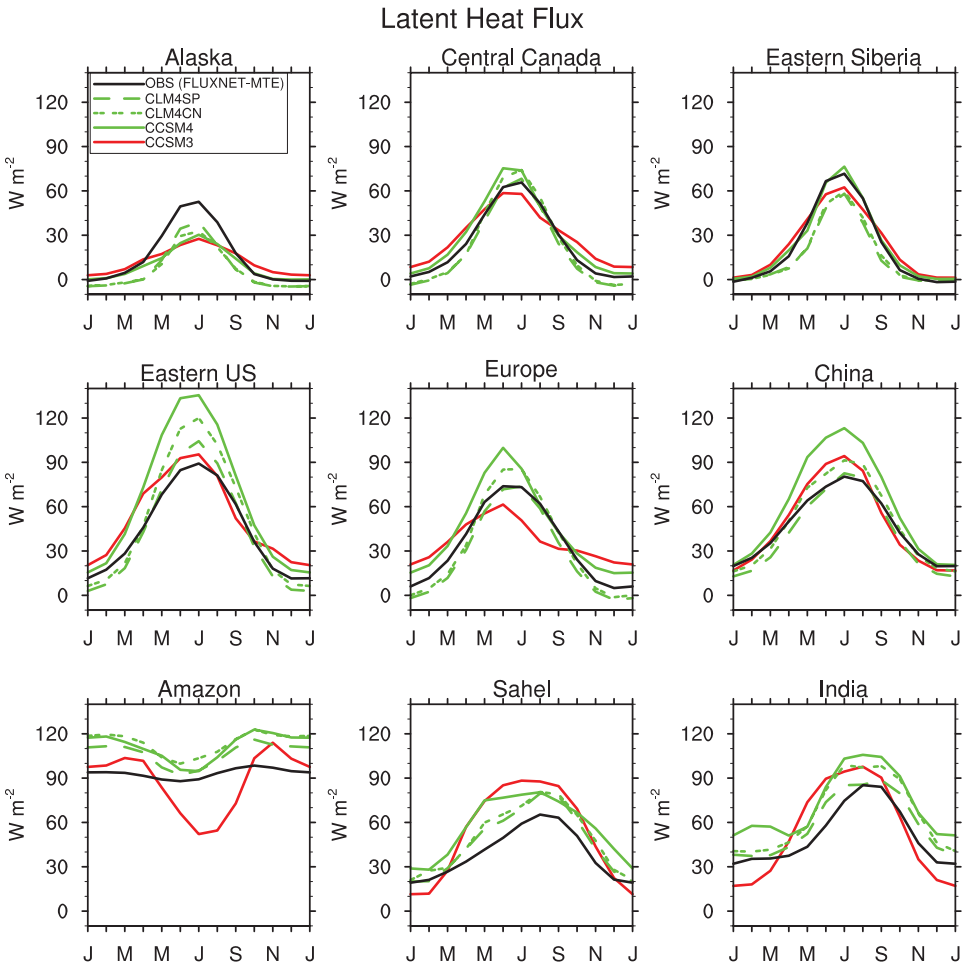

FIG. 5. Climatological (1980–99) annual cycle of latent heat flux for selected regions for CCSM3, CCSM4, and two offline CLM simulations (CLM4CN and CLM3) as well as observational estimates from FLUXNET-MTE. FLUXNET-MTE is from the FLUXNET network eddy covariance towers upscaled to monthly evapotranspiration on a 0.5° × 0.5° grid (Jung et al. 2010) using the model tree ensemble (MTE) approach described by Jung et al. (2009) (1982–2004 average). Regions defined as in Fig. 2.

world's 10 largest rivers, significant improvement (defined here as more than 50% reduction in bias) in the annual discharge is seen in CCSM4 for the Orinoco, Changjiang, and Brahmaputra–Ganges Rivers. None of the 10 largest rivers are significantly worse in CCSM4 than in CCSM3.

c. *Surface albedo, snow cover extent, and the snow albedo feedback*

The representation of surface albedo is improved in CCSM4 as a consequence of parameter adjustments, surface dataset updates, and parameterization changes in CLM4 that are discussed in Lawrence et al. (2011). The global mean bias in all-sky snow-free surface albedo compared to Moderate Resolution Imaging Spectroradiometer (MODIS) albedo estimates is reduced from +0.5% in CCSM3 to 0.0% in CCSM4 and the centered RMSE is reduced from 5.8% in CCSM3 to 2.1% in CCSM4. The MODIS all-sky albedo is derived from the black-sky (direct) and white-sky (diffuse) near-infrared and visible wave band albedos by weighting them according to the CCSM partitioning of solar radiation into these components. MODIS data are from collection 4 and are the climatological average of years 2001–2003.

Snow cover area and snow cover fraction, which together exert strong control on winter and spring surface albedo, suffered from seasonal biases in CCSM3 and are much improved in CCSM4 mainly due to a revised snow cover fraction (SCF) parameterization (Niu and Yang 2007) in CLM4. The Northern Hemisphere annual mean snow-covered area (SCA) bias is only +0.2/−0.7 million km^2 in CCSM4/CLM4 (19.6 million km^2 average) and is −4.2/−5.7 million km^2 in CCSM3/CLM3 (Table 1).

The representation of surface albedo and snow cover extent is important in a climate model since one of the

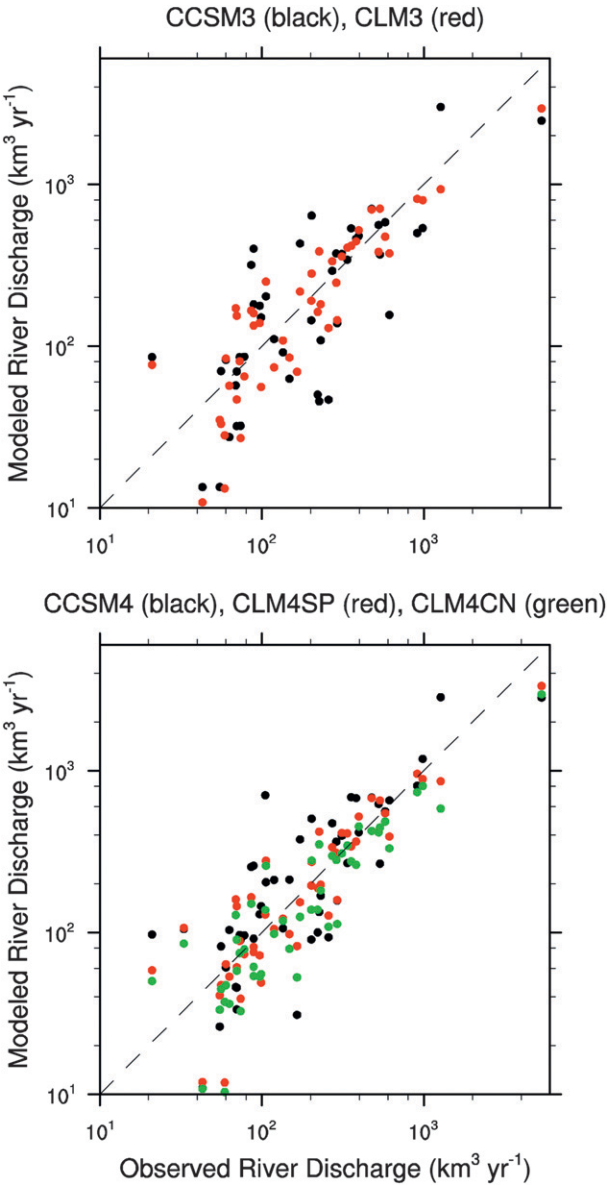

FIG. 6. Comparison of observed and modeled annual discharge for the world's largest 50 rivers for (top) CCSM3 and CLM3 and (bottom) CCSM4, CLM4CN, and CLM4SP. The Niger and Zambeze Rivers are excluded because the observed discharge is unrealistically low (Qian et al. 2006). Observed discharge is from Dai and Trenberth (2002).

primary mechanisms through which the land affects global climate sensitivity is through the snow albedo feedback (SAF; defined as the variation in absorbed solar radiation with T_{air} due to changes in surface albedo). Hall and Qu (2006) showed that the strength of SAF differs widely across the models that participated in the Coupled Model Intercomparison Project phase 3 (CMIP3; Meehl et al. 2007). Hall and Qu also found that the SAF in model projections of the twenty-first century can be accurately predicted by the model's representation of the SAF for the present-day annual cycle. Spring is the most important season for SAF (Hall 2004), and therefore it is important that the springtime [March–May (MAM)] mean climate is realistically simulated. CCSM4 has an improved representation of MAM surface albedo poleward of 30°N over snow-covered land [snow cover > 90%; bias of +0.9% in CCSM4, −3.1% in CCSM3 compared to Advanced Very High Resolution Radiometer (AVHRR) (Wang and Key 2005)] and snow-free land. The low bias in MAM snow cover fraction and the associated warm bias in MAM Arctic T_{air} in CCSM3 are largely eliminated in CCSM4.

The improvements to the model climatology and snow albedo in CCSM4 have a significant impact on the NH average SAF and lead to an overall improvement relative to CCSM3 (Fig. 7). The magnitude of total SAF in CCSM4 is reduced by ~25% compared to CCSM3, which brings it much closer to the observed value of $-1.07\%\ K^{-1}$. CCSM4 is also more realistic in representing the different components contributing to SAF. The component related to the albedo contrast between snow-covered and nonsnow-covered areas (SAF_{CON}) is almost twice as strong in CCSM4 as CCSM3 and closer to observed. This improvement is explained by (i) a stronger sensitivity of snow cover changes to hemispheric surface warming and (ii) the larger contrast between snow and land albedos in CCSM4.

The SAF_{ALB} term represents the component of SAF associated with snow aging, snow darkening, and physical transformations to the snowpack such as changes in grain size with temperature. CCSM4 is again in closer agreement with observations than CCSM3. Furthermore, CCSM4 realistically simulates SAF_{ALB} as a lower-order component of total SAF (Qu and Hall 2007), whereas in CCSM3 SAF_{ALB} is almost twice as strong as SAF_{CON}.

d. Twentieth-century simulations

Figure 8 shows time series of the global land temperature anomaly calculated relative to the mean of the years 1961–1990 for CCSM4 and CCSM3 compared against the CRUTEM3 observational estimate (Brohan et al. 2006). The models track the temperature time series well except that, as noted in Gent et al. (2011), the models simulate deep dips in temperature after Krakatoa and several other volcanoes in the late nineteenth and early twentieth century that are not recorded in the observations. The total simulated warming over land since the late nineteenth century (1980–99 minus 1880–99) exceeds that in the observations by about +0.3°C in CCSM4 (+0.2°C in CCSM3). This reflects the slightly too large top-of-atmosphere imbalance by 2005 in CCSM4, which may be due the lack of a representation of the indirect effects of aerosols in CCSM4 (Gent et al. 2011).

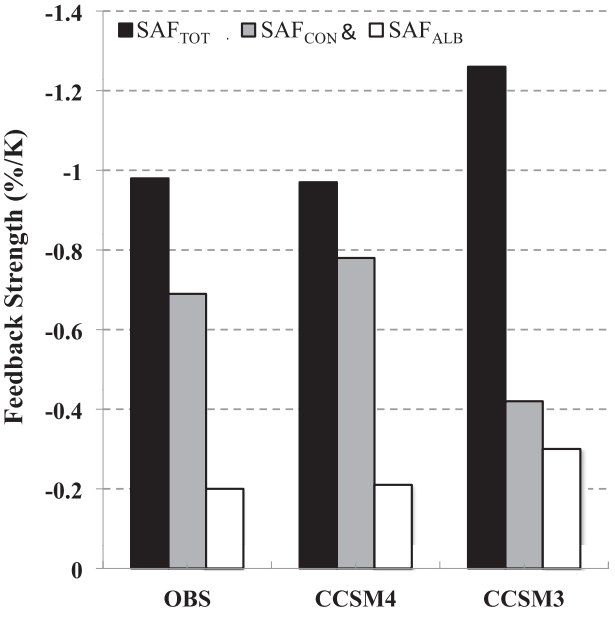

FIG. 7. Springtime (MAM) mean snow albedo feedback components derived from the climatological annual cycle 1982–99 (expressed in percent surface albedo change per degree Kelvin change, and estimated over Northern Hemisphere land areas poleward of 30°N). The total feedback (SAF_{TOT}, black) is the total sensitivity of changes in surface albedo to changes in surface temperature. SAF_{TOT} is decomposed into two physically distinct components: (i) the albedo contrast between snow-covered and snow-free surfaces (SAF_{CON}, gray); and (ii) variations in the albedo of snow-covered surfaces as a function of temperature (SAF_{ALB}, white). SAF_{CON} and SAF_{ALB} are computed using Eq. (18) from Qu and Hall (2007); however, instead of using their linear inversion technique to compute snow and land albedos, we use the direct method of Fernandes et al. (2009), which removes the constraint from Qu and Hall (2007) that $SAF_{TOT} \equiv SAF_{CON} + SAF_{ALB}$. The observational estimates are derived using surface albedo and snow cover data from the AVHRR Polar Pathfinder (APP-x) (Wang and Key 2005), and surface temperatures are from the National Centers for Environmental Prediction (NCEP)–Department of Energy (DOE) reanalysis (Kalnay et al. 1996).

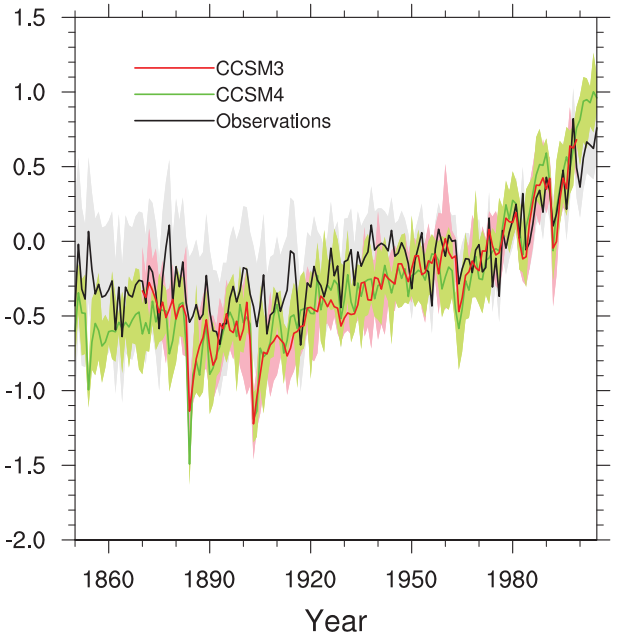

FIG. 8. Global land temperature anomaly time series for CCSM3 and CCSM4 compared against the CRUTEM3 observational estimate (Brohan et al. 2006). Anomalies are relative to the 1961–90 average for both model and observations. Shading for models shows range across the ensemble. Gray shading for observations is an estimate of the total observational uncertainty.

The stronger than observed land warming may also be partly related to the stronger than observed temperature response to the 1883 Krakatoa volcanic eruption, which brings the CCSM4 1880–99 mean T_{air} down considerably.

4. Earth system model features

a. *Climate in urban areas*

The addition of an urban surface type into CLM4 allows for simulation of the urban environment, including the temperature of cities, which is critical because the majority of people live in urban areas. In particular, the urban heat island, a phenomenon in which cities are warmer than their surrounding rural environs, can be examined using the urban model. Figure 9 compares the urban heat island (defined here as the difference in T_{air} between urban and rural surfaces in each grid cell) with the change in climate across the twentieth century simulated by CCSM4. The simulated annual mean present-day heat island ranges from 1°C in Central America to 2°C in eastern North America (NA). Oleson et al. (2010a) found that the heat island is predominantly a nocturnal phenomenon and is due to the urban area storing more heat during the day and then releasing this heat at night, thereby keeping urban surfaces warmer than rural surfaces at night. Urban latent heat is less than rural latent heat due to the presence of impervious surfaces, which also contributes to warmer urban temperatures. It is noteworthy that the present-day heat island is similar to or exceeds the simulated twentieth-century regional changes in T_{air} that range from 0.7°C in Europe to 1.1°C in western North America. Put another way, people moving from a rural to an urban area will experience a change in climate that is comparable to or greater than that which has occurred over the last 130 years or so. This argues for explicit representation of urban areas within climate models.

b. *Transient land cover and land use change impact on climate*

To isolate the biogeophysical and biogeochemical impacts of land use in CLM4 in the absence of other

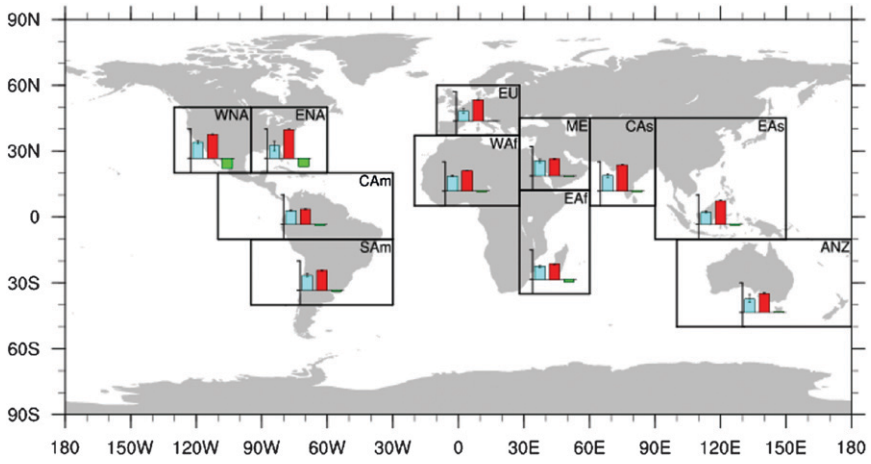

FIG. 9. CCSM4 ensemble annual mean of 1986–2005 minus 1850–69 T_{air} (blue bars), the present-day (1986–2005) urban heat island (red bars), and 1985–2004 minus 1850–69 $T_{air,LULC}$ derived from land cover/land use change only experiment (green bars). The urban heat island for each region is calculated as the difference between the regionally averaged T_{air}'s for urban and rural (vegetated and bare soil) surfaces. The T_{air} for urban is the urban canopy layer air temperature, and T_{air} for rural is the area-weighted average of the 2-m air temperature of the PFTs (including bare soil). Urban extent and urban properties are fixed at present-day conditions (Oleson 2012). In these simulations, urban areas occupy about 0.6% of the global land surface. Urban area is typically a small percentage of the land fraction of the grid cells (0.1%–10%) but may occupy up to 100% in coastal grid cells with a small land fraction. An analysis of changes in the heat island and urban model evaluation efforts are summarized in Oleson (2012). Vertical tickmarks are −1°, 0°, and 2°C. Western North America (WNA), Central America (CAm), South America (SAm), eastern North America, (ENA), Europe (EU), western Africa (WAf), Middle East (ME), eastern Africa (EAf), central Asia (CAs), eastern Asia (EAs), Australia/New Zealand (ANZ) (regions defined as in McCarthy et al. 2010). Ensemble range is shown for the regional twenty-first century climate warming and urban heat island bars. The urban heat island ensemble range is small enough for most regions so as not to be visible.

climate forcings, a supplementary land cover–land use change (LCLUC)-only twentieth-century simulation was performed with CCSM4. An illustration of the biogeophysical impact of historical LCLUC is shown in Fig. 9 where the regionally averaged surface air temperature change due to LCLUC ($\Delta T_{air,LCLUC}$; 1985–2004 minus 1850–69) is shown as an additional bar that can be compared to the total ΔT_{air} due to all forcings and the present day urban heat island. The regionally averaged $\Delta T_{air,LCLUC}$ is smaller and of opposite sign to the all forcing regional ΔT_{air} signal seen in CCSM4. The regional analysis also indicates that only in North America is the biogeophysical impact of LCLUC of similar magnitude to the combined climate forcings, with western North America exhibiting a −0.7°C LCLUC cooling against an overall warming of 1.1°C, and eastern North America exhibiting a −0.6°C cooling against overall warming of 0.9°C. The biogeochemical impact of LCLUC is discussed in section 4e.

c. *Radiative forcing due to black carbon and dust deposition onto snow*

Radiative forcing from black carbon (BC) and dust deposition to snow was simulated in CCSM4 with the SNICAR module (Flanner et al. 2007, 2009). Deposition fields were simulated in a separate transient chemical transport version of CCSM4 (Lamarque et al. 2010). Annual-mean terrestrial surface forcings for preindustrial (1850–69) and present-day (1986–2005) time periods are listed in Table 2. The snow particle forcings peak during boreal spring when snow cover and Northern Hemisphere insolation are both large (e.g., Flanner et al. 2009). Forcing on perennial snow surfaces like Greenland, however, peaks during the solstice season. Spatial patterns of forcings during March–May (MAM) are shown in Fig. 10. The present-day terrestrial MAM BC + dust forcing is 0.17 W m^{-2} and the effect averaged only over snow covered regions is 1.5 W m^{-2}.

TABLE 2. Global annual-mean radiative forcing of particles in land-based snowpack (W m^{-2}).

Species	Preindustrial (1850–69)	Present (1986–2005)
Black carbon	0.023	0.037
Mineral dust	0.046	0.036
Combined effect	0.075	0.083

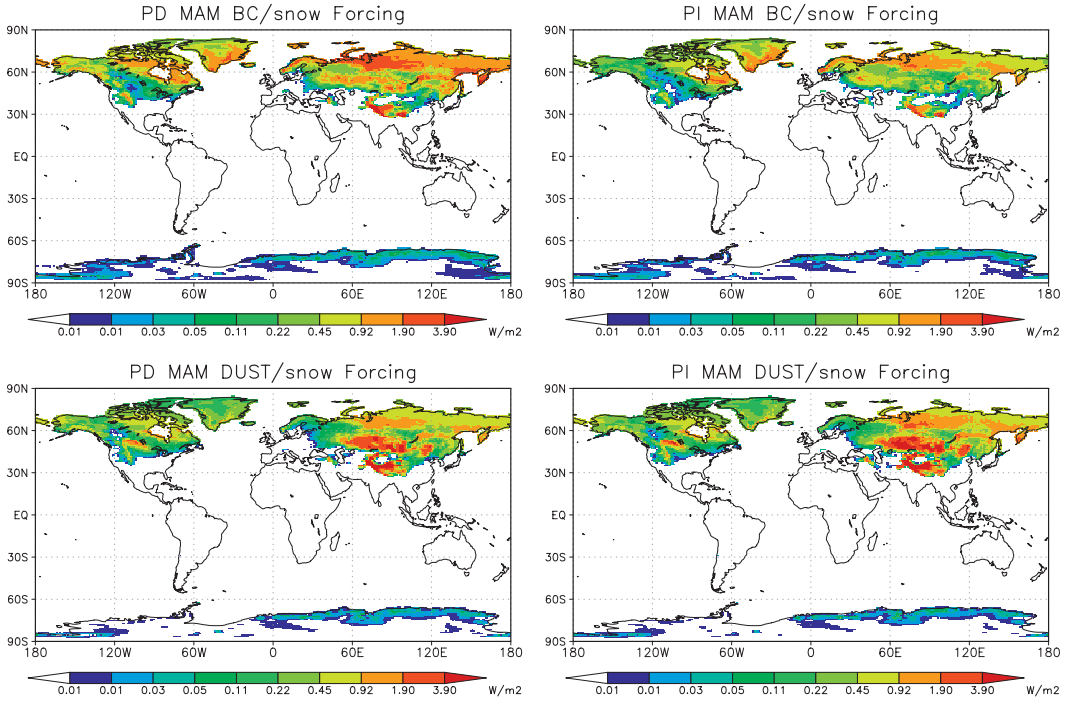

FIG. 10. Maps of (left) present day (PD, 1986–2005) and (right) preindustrial (PI, 1850–1869) spring (MAM) radiative forcing of (top) black carbon and (bottom) dust on snow in CCSM4. Note that the scale is logarithmic.

The combined BC + dust forcing is 13% greater than the sum of their individual forcings, manifesting some nonlinearity in forcing. Here, BC forcing is calculated as the change in solar absorption when BC is removed from the snowpack (while leaving dust), and likewise dust forcing represents the effect of removing dust (while leaving BC).

Snow forcing from BC during the midnineteenth century was more than half as large as the present-day forcing. Preindustrial BC emissions are substantial in the inventory applied (Lamarque et al. 2010) to simulate aerosol deposition. Open burning (natural) emissions were about 2 Tg yr^{-1} in 1860, only slightly smaller than present, and anthropogenic sources were about 1.25 Tg yr^{-1}. These compare with total 2000 emissions of 7.6 Tg yr^{-1}. Normalizing the global BC/snow forcings to emissions, however, indicates that preindustrial emissions were more effective than present emissions at darkening snow. One reason for this is greater snow coverage in the preindustrial state, which increased the available surface area for forcing. Excluding Greenland and Antarctica, annual-mean snow cover decreased by about 8% between these two time periods. A second reason for greater preindustrial normalized forcing may relate to the different spatial–temporal patterns of preindustrial BC deposition. Another interesting feature is that BC and dust snow forcings are about equal in the present day. This is in contrast to an earlier study with CAM3 (Flanner et al. 2009), where BC–snow forcing was more than double dust–snow forcing. The difference can be attributed mostly to much greater Asian dust emissions and deposition in the current study. Land-averaged BC–snow forcing decreased slightly from 0.040 to 0.037 W m^{-2} between these studies, due to application of new emissions (Lamarque et al. 2010), whereas dust–snow forcing increased from 0.019 to 0.036 W m^{-2}. Dust–snow forcing decreased in this study by about 20% from the preindustrial to present states. In the deposition fields applied, global land-averaged dust deposition was nearly the same in 1850–69 and 1986–2005, indicating again that greater preindustrial snow coverage facilitated greater forcing.

d. Permafrost

The representation of permafrost, which was crude in CCSM3, is improved in CCSM4 because of several improvements in the CLM soil model, especially the explicit accounting for the thermal and hydrologic properties of organic soil and an extension of the ground column to ~50-m depth (Lawrence et al. 2008). Maps of present-day near-surface permafrost extent and active-layer thickness (ALT, defined as the depth to which soil thaws in the summer) are shown in Fig. 11. A grid cell has near-surface permafrost if one of the top 10 soil

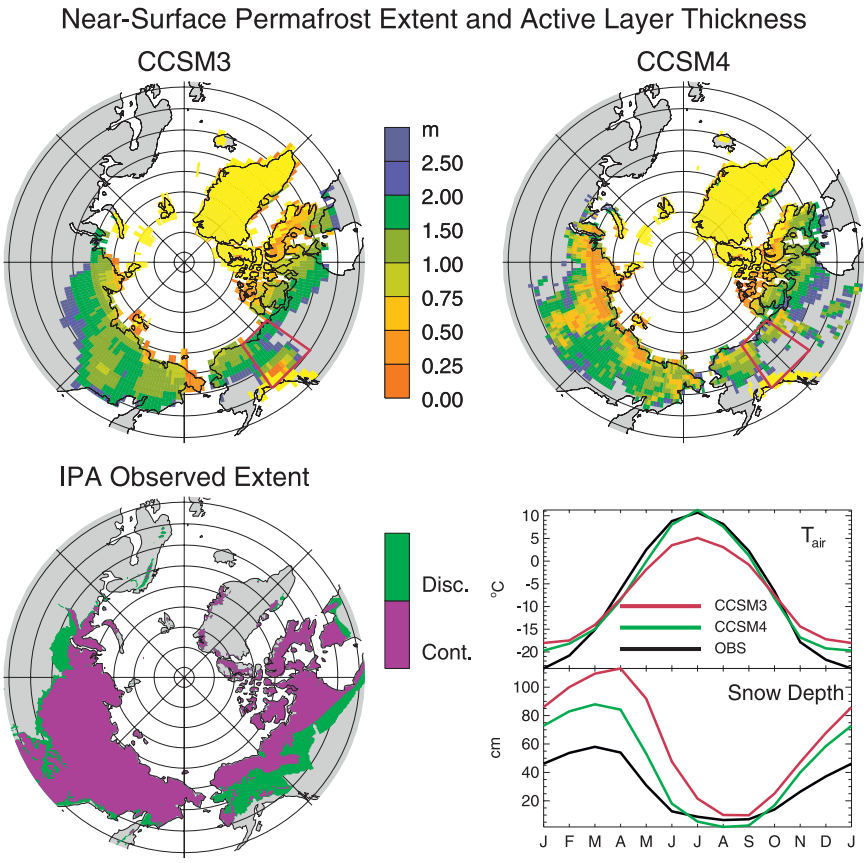

FIG. 11. (top) Maps of diagnosed near-surface permafrost extent (colored area) and active-layer thickness in (left) CCSM3 and (right) CCSM4 (1980–99). Bright yellow indicates that grid cell is predominantly a glacier land type. (bottom) (left) Observational estimate of continuous and discontinuous permafrost distribution is from the IPA map (Brown et al. 1998). (bottom right) The climatological annual cycle of T_{air} and snow depth for the boxed eastern Alaska/western Canada region for the years 1980–99 is shown. The T_{air} observational data are from (Matsuura and Willmott 2009b). The snow depth climatology observational data are from the Canadian Meteorological Center (1980–96) (Brown et al. 2003).

levels (bottom of layer 10 depth is ~3.5 m) remains frozen ($T_{soil} < 0°C$) for the entire year. In both CCSM4 and CCSM3, the spatial pattern and extent of present-day near-surface permafrost is reasonably simulated, which is a reflection of the quality of the simulated Arctic climate, though errors can be identified in both model versions. The spatial distribution of near-surface permafrost and its integrated area can be qualitatively compared to maps of continuous and discontinuous permafrost provided by the International Permafrost Association (IPA, Brown et al. 1998). Continuous and discontinuous permafrost denote regions in which 90%–100% and 50%–90%, respectively, of a given area is underlain by permafrost. Though a direct comparison with the IPA maps is difficult because each model grid cell is either identified as permafrost or not (i.e., there is no subgrid-scale representation of permafrost distribution), the spatial pattern and extent appears to be slightly improved in CCSM4—11.2 million km^2 compared to 10.5 million km^2 in CCSM3 compared to observed estimates of 11.1 to 14.9 million km^2 (Zhang et al. 2000).

There are two main regions where near-surface permafrost is erroneously absent in CCSM4, southern Siberia and eastern Alaska–western Canada. In the latter region, permafrost is absent in CCSM4 but correctly exists in CCSM3. It is interesting to note that the model does not generate permafrost in eastern Alaska–western Canada in CCSM4 even though the climate simulation in this region appears to be improved (see lower right panel in Fig. 11). The cool summer T_{air} bias seen in CCSM3 is eliminated in CCSM4 and the excessive snow depth (due to excessive snowfall) bias in CCSM3 is also reduced, though not completely eliminated. It appears that compensating errors in CCSM3 (cool summer T_{air} combined

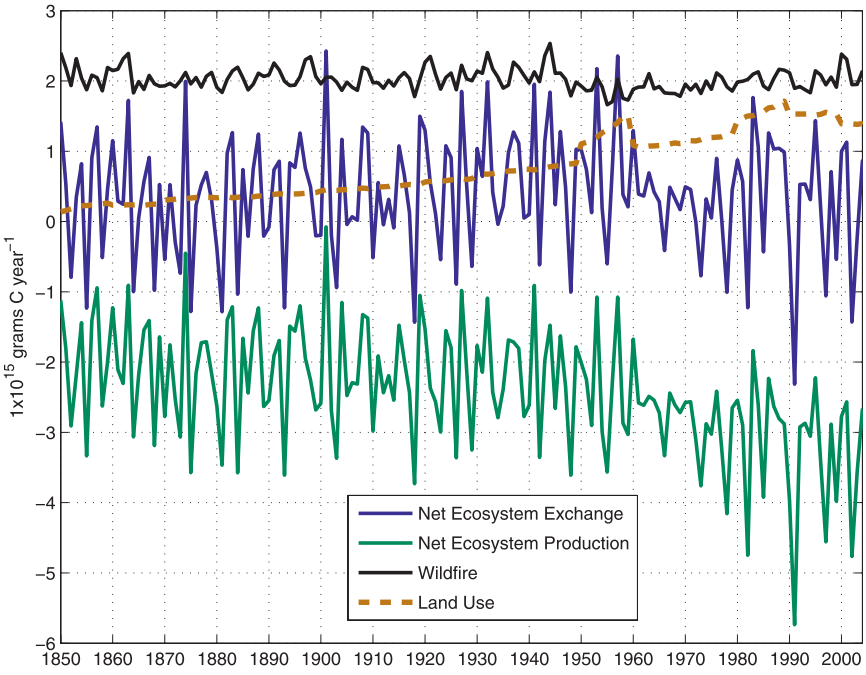

FIG. 12. Simulated time series of land carbon fluxes from a single 1850–2004 CCSM4 simulation. Net ecosystem exchange is sum of net ecosystem production, wildfire, and land use fluxes. A positive value represents a source to the atmosphere. For net ecosystem production we have reversed the standard sign convention to make the figure easier to interpret.

with a too deep, and therefore too insulating, winter snowpack) combined to maintain near-surface permafrost in this region. Apparently, even though the cool summer T_{air} bias is no longer a problem in CCSM4, the excessive snow depths in the winter keep the ground warmer than it should be and prevents permafrost from existing in this region.

The ALT (the depth to which the soils thaw each summer) is also more realistic in CCSM4. In CCSM3, the ALT is fairly uniform across the permafrost domain and is generally thicker than has been observed through the Circumpolar Active Layer Monitoring network (Brown et al. 2000). Accounting for the insulating properties of organic soil tends to reduce soil temperatures and generates generally shallower and more realistic ALTs. Further analysis of the representation of permafrost and projections of future permafrost including comparisons against observed ALT and deep ground temperatures and the impact of CCSM4 climate biases on present-day and future permafrost are presented in D. M. Lawrence et al. (2012).

e. *Terrestrial carbon fluxes*

A major new feature of CLM4 is the inclusion of a prognostic CN cycle model. When the CN model is active in CLM, as it is for the simulations evaluated here, the model calculates diagnostic fluxes of carbon and nitrogen according to the climate and vegetation for each grid cell. Time series of land carbon fluxes from one of the CCSM4 ensemble members are shown in Fig. 12. Note that in these CCSM4 simulations, atmospheric CO_2 is prescribed and therefore the atmosphere does not see these fluxes. Separate simulations are being conducted with a fully prognostic global carbon cycle.

By convention, a positive net ecosystem exchange (NEE) indicates a source of CO_2 from the land to the atmosphere. NEE in CLM4 is the sum of CO_2 fluxes due to land use (defined as the direct emission of carbon to the atmosphere from changing land cover, e.g., conversion of forests to cropland or vice versa, and wood harvest), wildfire, and net ecosystem production (NEP). CLM4 simulates increasing ecosystem uptake from 1850 to 2004 as a result of increasing atmospheric CO_2 and increasing nitrogen deposition, which both tend to fertilize vegetation (Bonan and Levis 2010). Land use is an increasing source of CO_2 at levels that agree with the end of the twentieth-century observational estimates (Bonan and Levis 2010). Wildfire shows no perceptible trend and the values agree with those from a comprehensive fire modeling study with CLM (Kloster et al. 2010). As a result of the three contributing fluxes (land use, wildfire, and NEP), NEE remains on average slightly

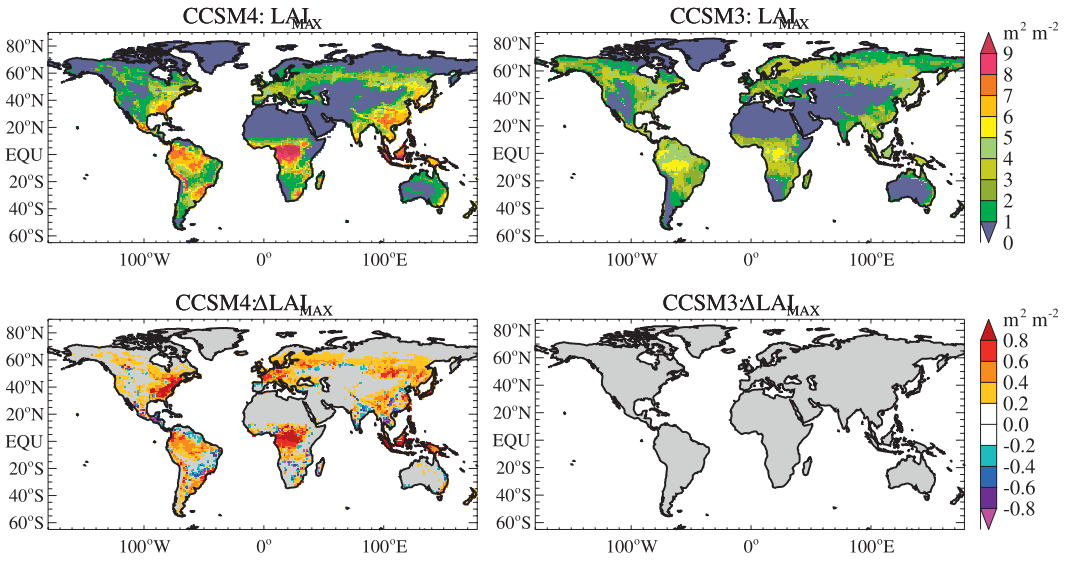

FIG. 13. (top) Ensemble mean–simulated annual maximum monthly LAI for (left) CCSM4 and prescribed annual maximum LAI for (right) CCSM3. (bottom) Ensemble-mean simulated change (1980–99 minus 1880–99) in monthly maximum LAI in (left) CCSM4; LAI change is zero by definition in (right) CCSM3. LAI in each grid cell is the PFT area-weighted mean.

positive throughout the simulation meaning that natural and anthropogenic terrestrial processes are a small source of CO_2. This flux would represent an additional source of carbon to the atmosphere, on top of the fossil fuel combustion source. X. Lindsay et al. (2011, unpublished manuscript) and P. Thornton et al. (2011, unpublished manuscript) will investigate whether or not this net source of carbon from the land to the atmosphere is also seen in a fully coupled carbon cycle simulation with interactive CO_2.

f. Prognostic vegetation state: Trends and impact of variability on climate

In CCSM3 the vegetation state [LAI; stem area index (SAI); and canopy height] is prescribed (Bonan et al. 2002a) and does not vary on interannual time scales. In CCSM4, the vegetation state is prognostic, which means that the timing of vegetation greening and senescence varies from year to year according to the simulated climate. Additionally, the annual maximum LAI varies over time in response to changes in atmospheric CO_2 levels, nitrogen deposition, and climate. Prescribed land cover change and wood harvest also affects vegetation state. LAI, SAI, and canopy height have a direct impact on climate through biogeophysical feedbacks related to surface roughness and momentum transfer, canopy interception and evaporation, transpiration, and surface albedo.

Figure 13 shows the simulated annual maximum LAI for CCSM4 and the prescribed observed maximum LAI for CCSM3. Simulated LAI is high in CCSM4 across the tropics and midlatitudes. LAI is low in the northern high latitudes, probably due to the dry soil moisture bias (Section 3b). Also shown in Fig. 13 is the change in annual maximum LAI from the end of the nineteenth century to the end of the twentieth century for CCSM4. Increases of up to 1 m^2 m^{-2} are seen in many regions including tropical Africa, Amazonia, Indonesia, eastern North America, Europe, and across the Asian boreal forest. Modest decreases in LAI are seen in southeast Brazil and India.

The introduction of a prognostic phenology model can alter the interannual variability of surface climate through the modulating impact of vegetation state on surface fluxes. Changes in variability (defined here as the standard deviation of monthly 100-yr anomaly time series from a preindustrial control run) for T_{air}, LH, and LAI are shown in Fig. 14 for two sets of models: CCSM4SP (CCSM4 with satellite prescribed rather than prognostic vegetation phenology) compared to CCSM3 and CCSM4 compared to CCSM4SP. Considering first the CCSM4SP–CCSM3 pair of models (left panels, Fig. 14; LAI does not vary interannually in either model), LH and T_{air} variability decreases across most of the tropics and subtropics. This is a result of the generally moister soils and consequently less frequent occurrence of soil moisture stress on photosynthesis and transpiration in CCSM4. Variability in T_{air} increases across the high latitudes due to increased variation in the timing of snowmelt.

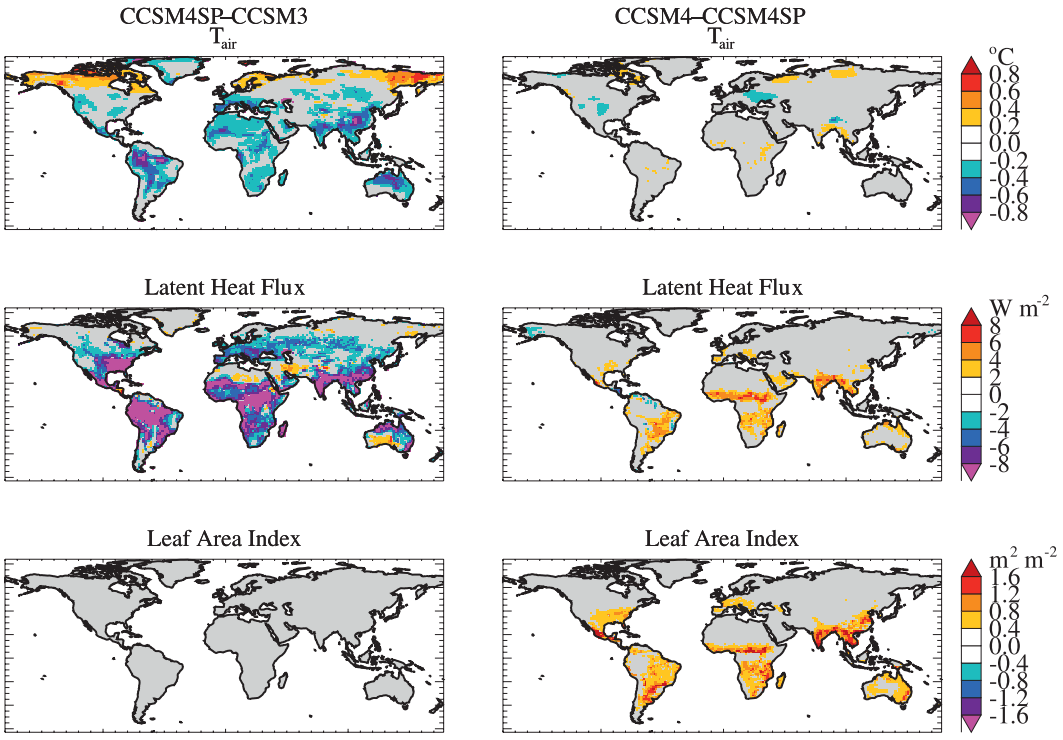

FIG. 14. Change in variability of (top to bottom) T_{air}, LH, and LAI from (left) CCSM3 to CCSM4SP and (right) CCSM4SP to CCSM4. Variability is calculated as the standard deviation of the monthly anomaly time series from a 100-yr segment of the preindustrial control for each integration.

Latent heat flux variability increases in CCSM4 compared to CCSM4SP (right panels, Fig. 14), increasing in regions in which LAI variability in CCSM4 is high. An evaluation of the monthly annual cycle of LH and LAI standard deviations in CLM4CN for selected regions (Lawrence et al. 2011) indicates that the variability increase is associated with both enhanced growing season LAI variability and variations in the timing of leaf on and off.

5. Summary and discussion

Overall, the surface climate is better simulated in CCSM4 than in CCSM3, although some features are degraded. Where offline analyses indicate an improvement in CLM4 compared CLM3 or CLM3.5 (e.g., soil water storage, evapotranspiration, surface albedo, and soil temperature), the improvement typically carries over into the coupled simulation. For variables such as air temperature and precipitation, which depend on interacting processes that are influenced by all components of the coupled model system, the improvements are less uniform. The global land-averaged-centered RMSE is lower for both surface air temperature and precipitation, by about 20% and 5% respectively, which indicates a general improvement in the simulation of the annual cycle for both variables. Regionally, the biggest surface air temperature bias in CCSM4 is a +2° to +4°C annual mean warm bias over Europe and western Asia (see Fig. 10, Gent et al. 2011). Experiments with the Community Atmosphere Model, version 3.5 (CAM3.5)–CLM3.5 that included irrigation exhibited cooling across this region (Sacks et al. 2009), which suggests that including irrigation could potentially alleviate part of this warm bias. For precipitation, there is excessive annual mean precipitation (+1 to +2 mm day^{-1}) in CCSM4 across most of southern and central Africa and Australia. Significant biases (+0.2 to 1.0 mm day^{-1}) are also apparent across much of the northern high latitudes; especially relevant is the excessive snowfall that leads to deeper snowpacks than observed. Because of the insulating properties of snow, an erroneously deep snowpack can shift soil temperatures warmer and in some situations prevent permafrost from existing where it otherwise would, based on simulated air temperature (see Fig. 11).

In this paper, we introduce and provide initial assessments of several new capabilities of the land model within the CCSM4 modeling system. Several of these aspects will be evaluated in greater detail in other papers within the CCSM4 Journal of Climate Special Collection. The urban canyon model permits the study of the impact of

climate change in urban environments (Oleson 2012). The prescription of transient historical land cover and land use change increases the realism of the representation of the land surface and provides insights into the impact of land cover and land use change on biogeophysical and biogeochemical processes (Lawrence et al. 2012). Aerosol deposition onto snow represents a newly represented forcing of the climate system. A more realistic and complete representation of permafrost paves the way for subsequent study of the impact of projected permafrost thaw on terrestrial Arctic feedbacks. The addition of a carbon and nitrogen cycle model allows a diagnostic analysis of terrestrial carbon fluxes and their evolution due to land use, wildfire, and changes in net ecosystem production due to climate change.

The incorporation of CN and its prognostic vegetation phenology scheme, in particular, adds an important and realistic degree of freedom to the CCSM4 simulations through the capacity to represent interannual variations in vegetation phenology and structure. It is important to keep in mind, however, that the addition of this extra degree of freedom tends to degrade the mean biogeophysical simulation, as discussed in Lawrence et al. (2011). The simulated LAI in CCSM4 (and CLM4CN) appears to be biased high across much of the world, and this high LAI bias leads to excessive transpiration (Fig. 5), which affects the partitioning of the surface turbulent fluxes and consequently the atmospheric boundary layer and reduces the amount of water available for runoff and discharge to the oceans. Additionally, although not discussed here, the phenology scheme that determines vegetation greening and senescence dates, though reasonably represented for some regions, requires additional assessment and improvement (Lawrence et al. 2011). The unrealistically high evapotranspiration in CCSM4 is not solely a function of excessive LAI. As noted in section 3b, an evaluation of the photosynthesis model that has occurred since the release of CCSM4–CLM4 revealed structural errors in canopy radiative transfer, leaf photosynthesis, and stomatal conductance models and model parameter errors in the photosynthetic parameter $V_{c,\max}$ (Bonan et al. 2011). Evapotranspiration rates are substantially improved in offline CLM4SP simulations with these problems corrected (Bonan et al. 2011).

Another significant problem for vegetation modeling in CCSM4 (and CLM4CN) is an apparent dry bias in permafrost soils with high organic matter. The dry soils appear to severely inhibit vegetation growth across much of the northernmost high latitudes resulting in very anemic LAI and other vegetation state parameters. Initial analysis indicates that the dry bias is related to a structural error in CLM4 that permits excessive soil water movement through icy soils. This problem is being addressed through a comprehensive revision of the CLM cold region hydrology parameterizations. Other aspects of the land hydrology simulation can also be improved. Soil moisture variability appears to be weaker than observed, especially near the surface, and the hydrographs of some major rivers, especially Arctic rivers, remain poorly simulated in both coupled and uncoupled simulations.

Finally, there are several projects in progress or recently completed that integrate unrepresented aspects of the land system into CLM including the addition of a crop model, an irrigation model (based on Sacks et al. 2009), a methane emissions model (Riley et al. 2011), a prognostic wetland distribution scheme, water and carbon isotopes, and ecosystem demography concepts (based on Fisher et al. 2010). Efforts are also ongoing across the CLM development community to improve existing parameterizations, including projects on vegetation and soil carbon dynamics, nitrogen dynamics, lake-model thermodynamics (Subin et al. 2012), cold region hydrology, subgrid soil moisture and snow, and more advanced river discharge modeling. Work is also underway to improve parameterizations and parameter settings in a more objective way through data assimilation of flux tower data.

Acknowledgments. The CCSM/CESM project is supported by the NSF and the Office of Science (BER) of the U.S. Department of Energy. Computing resources were provided by the Climate Simulation Laboratory at NCAR's Computational and Information Systems Laboratory (CISL), sponsored by NSF and other agencies. This research was enabled by CISL compute and storage resources. Bluefire, a 4064-processor IBM Power6 resource with a peak of 77 TeraFLOPS provided more than 7.5 million computing hours, the GLADE high-speed disk resources provided 0.4 PetaBytes of dedicated disk and CISL's 12-PB HPSS archive provided over 1 PetaByte of storage in support of this research project. Several model integrations were also performed at the Oak Ridge Leadership Computing Facility, which is supported by the Office of Science of the U.S. Department of Energy under Contract DE-AC05-00OR22725. Thanks are due to the many software engineers and scientists who contributed to the development of CCSM4. In particular, we would like to acknowledge the invaluable contribution of Erik Kluzek, the primary CLM software engineer. CLM4 development benefitted from substantial input of members of the CCSM Land Model and Biogeochemistry Working Groups. Gordon Bonan (NCAR), David Lawrence (NCAR), Keith

Lindsay (NCAR), Natalie Mahowald (Cornell University), Jim Randerson (UC Irvine), Steve Running (University of Montana), and Zong-Liang Yang (University of Texas at Ausin) were co-chairs of the LMWG and BGCWGs during the development of CLM4. DML is supported by funding from the U.S. Department of Energy BER, as part of its Climate Change Prediction Program, Cooperative Agreement DE-FC03-97ER62402/A010. MGF supported by NSF ATM-0852775.

REFERENCES

Bonan, G. B., and S. Levis, 2010: Quantifying carbon–nitrogen feedbacks in the Community Land Model (CLM4). *Geophys. Res. Lett.,* **37,** L07401, doi:10.1029/2010GL042430.

——, ——, L. Kergoat, and K. W. Oleson, 2002a: Landscapes as patches of plant functional types: An integrating concept for climate and ecosystem models. *Global Biogeochem. Cycles,* **16,** 1021, doi:10.1029/2000GB001360.

——, K. W. Oleson, M. Vertenstein, S. Levis, X. B. Zeng, Y. J. Dai, R. E. Dickinson, and Z. L. Yang, 2002b: The land surface climatology of the community land model coupled to the NCAR community climate model. *J. Climate,* **15,** 3123–3149.

——, P. J. Lawrence, K. W. Oleson, S. Levis, M. Jung, M. Reichstein, D. M. Lawrence, and S. C. Swenson, 2011: Global FLUXNET diagnostic models improve canopy processes in the Community Land Model (CLM4). *J. Geophys. Res.,* **116,** G02014, doi:10.1029/2010JG001593.

Branstetter, M. L., and J. S. Famiglietti, 1999: Testing the sensitivity of GCM-simulated runoff to climate model resolution using a parallel river transport algorithm. Preprints, *14th Conf. on Hydrology,* Dallas, TX, Amer. Meteor. Soc., 6B.11. [Available online at http://ams.confex.com/ams/older/99annual/abstracts/851.htm.]

Brohan, P., J. J. Kennedy, I. Harris, S. F. B. Tett, and P. D. Jones, 2006: Uncertainty estimates in regional and global observed temperature changes: A new data set from 1850. *J. Geophys. Res.,* **111,** D12106, doi:10.1029/2005JD006548.

Brown, J., O. J. Ferrians, J. A. Heginbottom, and E. S. Melnikov, 1998: International permafrost association circum-Arctic map of permafrost and ground-ice conditions. U.S. Geological Survey, Circum-Pacific Map Series, Map CP-45, Scale 1:10 000 000. [Available online at http://www.nsidc.org.]

——, K. M. Hinkel, and F. E. Nelson, 2000: The Circumpolar Active Layer Monitoring (CALM) program: Research designs and initial results. *Polar Geogr.,* **24,** 165–258.

Brown, R. D., B. Brasnett, and D. Robinson, 2003: Gridded North American monthly snow depth and snow water equivalent for GCM evaluation. *Atmos.–Ocean,* **41,** 1–14.

Collins, W. D., and Coauthors, 2006: The Community Climate System Model, version 3 (CCSM3). *J. Climate,* **19,** 2122–2143.

Dai, A. G., and K. E. Trenberth, 2002: Estimates of freshwater discharge from continents: Latitudinal and seasonal variations. *J. Hydrometeor.,* **3,** 660–687.

Danabasoglu, G., S. Bates, B. P. Briegleb, S. R. Jayne, W. G. Large, S. Peacock, and S. G. Yeager, 2012: The CCSM4 ocean component. *J. Climate,* **25,** 1361–1389.

Dickinson, R. E., K. W. Oleson, G. Bonan, F. Hoffman, P. Thornton, M. Vertenstein, Z.-L. Yang, and X. Zeng, 2006: The Community Land Model and its climate statistics as a component of the Community Climate System Model. *J. Climate,* **19,** 2302–2324.

Fernandes, R., H. Zhao, X. Wang, J. Key, X. Qu, and A. Hall, 2009: Controls on Northern Hemisphere snow albedo feedback quantified using satellite Earth observations. *Geophys. Res. Lett.,* **36,** L21702, doi:10.1029/2009GL040057.

Fisher, R., and Coauthors, 2010: Assessing uncertainties in a second-generation dynamic vegetation model caused by ecological scale limitations. *New Phytol.,* **187,** 666–681.

Flanner, M. G., and C. S. Zender, 2005: Snowpack radiative heating: Influence on Tibetan Plateau climate. *Geophys. Res. Lett.,* **32,** L06501, doi:10.1029/2004GL022076.

——, and ——, 2006: Linking snowpack microphysics and albedo evolution. *J. Geophys. Res.,* **111,** D12208, doi:10.1029/2005JD006834.

——, ——, J. T. Randerson, and P. J. Rasch, 2007: Present-day climate forcing and response from black carbon in snow. *J. Geophys. Res.,* **112,** D11202, doi:10.1029/2006JD008003.

——, ——, P. G. Hess, N. M. Mahowald, T. H. Painter, V. Ramanathan, and P. J. Rasch, 2009: Springtime warming and reduced snow cover from carbonaceous particles. *Atmos. Chem. Phys.,* **9,** 2481–2497.

Gent, P. R., and Coauthors, 2011: The Community Climate System Model, version 4. *J. Climate,* **24,** 4973–4991.

Guenther, A., T. Karl, P. Harley, C. Wiedinmyer, P. I. Palmer, and C. Geron, 2006: Estimates of global terrestrial isoprene emissions using MEGAN (model of emissions of gases and aerosols from nature). *Atmos. Chem. Phys. Discuss.,* **6,** 107–173.

Hall, A., 2004: The role of surface albedo feedback in climate. *J. Climate,* **17,** 1550–1568.

——, and X. Qu, 2006: Using the current seasonal cycle to constrain snow albedo feedback in future climate change. *Geophys. Res. Lett.,* **33,** L03502, doi:10.1029/2005GL025127.

Heald, C. L., and Coauthors, 2008: Predicted change in global secondary organic aerosol concentrations in response to future climate, emissions, and land use change. *J. Geophys. Res.,* **113,** D05211, doi:10.1029/2007JD009092.

Holland, M. M., D. A. Bailey, B. P. Briegleb, B. Light, and E. C. Hunke, 2012: Improved sea ice shortwave radiation physics in CCSM4: The impact of melt ponds and aerosols on arctic sea ice. *J. Climate,* **25,** 1413–1430.

Hurtt, G. C., S. Frolking, M. G. Fearon, B. Moore, E. Shevliakova, S. Malyshev, S. W. Pacala, and R. A. Houghton, 2006: The underpinnings of land-use history: Three centuries of global gridded land-use transitions, wood-harvest activity, and resulting secondary lands. *Global Change Biol.,* **12,** 1208–1229.

Jung, M., M. Reichstein, and A. Bondeau, 2009: Towards global empirical upscaling of FLUXNET eddy covariance observations: Validation of a model tree ensemble approach using a biosphere model. *Biogeosciences,* **6,** 2001–2013, doi:10.5194/bg-6-2001-2009.

——, and Coauthors, 2010: Recent decline in the global land evapotranspiration trend due to limited moisture supply. *Nature,* **467,** 951–954, doi:10.1038/nature09396.

Kalnay, E., and Coauthors, 1996: The NCEP/NCAR 40-Year Reanalysis Project. *Bull. Amer. Meteor. Soc.,* **77,** 437–471.

Kloster, S., and Coauthors, 2010: Fire dynamics during the 20th century simulated by the Community Land Model. *Biogeosciences,* **7,** 1877–1902, doi:10.5194/bg-7-1877-2010.

Lamarque, J.-F., and Coauthors, 2010: Historical (1850–2000) gridded anthropogenic and biomass burning emissions of reactive gases and aerosols: Methodology and application. *Atmos. Chem. Phys. Discuss.,* **10,** 4963–5019, doi:10.5194/acpd-10-4963-2010.

Lawrence, D. M., and A. G. Slater, 2008: Incorporating organic soil into a global climate model. *Climate Dyn.,* **30,** doi:10.1007/s00382-007-0278-1.

——, and ——, 2010: The contribution of changes in snow conditions on future ground climate. *Climate Dyn.,* **34,** 969–981, doi:10.1007/s00382-009-0537-4.

——, P. E. Thornton, K. W. Oleson, and G. B. Bonan, 2007: Partitioning of evaporation into transpiration, soil evaporation, and canopy evaporation in a GCM: Impacts on land–atmosphere interaction. *J. Hydrometeor.,* **8,** 862–880.

——, A. G. Slater, V. E. Romanovsky, and D. J. Nicolsky, 2008: The sensitivity of a model projection of near-surface permafrost degradation to soil column depth and inclusion of soil organic matter. *J. Geophys. Res.,* **113,** F02011, doi:10.1029/2007JF000883.

——, and Coauthors, 2011: Parameterization improvements and functional and structural advances in version 4 of the Community Land Model. *J. Adv. Model. Earth Syst.,* **3,** doi:10.1029/2011MS000045.

——, A. G. Slater, and S. C. Swenson, 2012: Simulation of present-day and future permafrost and seasonally frozen ground conditions in CCSM4. *J. Climate,* **25,** 2207–2225.

Lawrence, P. J., and T. N. Chase, 2007: Representing a new MODIS consistent land surface in the Community Land Model (CLM3.0). *J. Geophys. Res.,* **112,** G01023, doi:10.1029/2006JG000168.

——, and Coauthors, 2012: Simulating the biogeophysical and biogeochemical impacts of land cover change and forestry in the Community Climate System Model (CCSM4). *J. Climate,* in press.

Levis, S., G. B. Bonan, M. Vertenstein, and K. W. Oleson, 2004: The Community Land Model's dynamic global vegetation model (CLM-DGVM): Technical description and user's guide. NCAR Tech. Note TN-459+IA, 50 pp.

Matsuura, K., and C. J. Willmott, cited 2009a: Terrestrial precipitation: 1900–2008 gridded monthly time series, version 2.01. [Available online at http://climate.geog.udel.edu/~climate/.]

——, and ——, cited 2009b: Terrestrial air temperature: 1900–2008 gridded monthly time series, version 2.01. [Available online at http://climate.geog.udel.edu/~climate.]

McCarthy, M. P., M. J. Best, and R. A. Betts, 2010: Climate change in cities due to global warming and urban effects. *Geophys. Res. Lett.,* **37,** L09705, doi:10.1029/2010GL042845.

Meehl, G. A., C. Covey, T. Delworth, M. Latif, B. McAvaney, J. F. B. Mitchell, R. J. Stouffer, and K. E. Taylor, 2007: The WCRP CMIP3 multimodel dataset—A new era in climate change research. *Bull. Amer. Meteor. Soc.,* **88,** 1383–1394.

Mitchell, T. D., and P. D. Jones, 2005: An improved method of constructing a database of monthly climate observations and associated high-resolution grids. *Int. J. Climatol.,* **25,** 693–712, doi:10.1002/joc.1181.

Neale, R. B., J. H. Richter, and M. Jochum, 2008: The impact of convection on ENSO: From a delayed oscillator to a series of events. *J. Climate,* **21,** 5904–5924.

Niu, G. Y., and Z. L. Yang, 2007: An observation-based formulation of snow cover fraction and its evaluation over large North American river basins. *J. Geophys. Res.,* **112,** D21101, doi:10.1029/2007JD008674.

Oleson, K. W., 2012: Contrasts between urban and rural climate in CCSM4 CMIP5 climate change scenarios. *J. Climate,* **25,** 1390–1412.

——, and Coauthors, 2004: Technical description of the Community Land Model (CLM). NCAR Tech. Note TN-461+STR, 174 pp.

——, G. B. Bonan, J. Feddema, M. Vertenstein, and C. S. B. Grimmond, 2008a: An urban parameterization for a global climate model. Part I: Formulation and evaluation for two cities. *J. Appl. Meteor. Climatol.,* **47,** 1038–1060.

——, and Coauthors, 2008b: Improvements to the Community Land Model and their impact on the hydrological cycle. *J. Geophys. Res.,* **113,** doi:10.1029/2007JG000563.

——, G. B. Bonan, J. Feddema, and T. Jackson, 2010a: An examination of urban heat island characteristics in a global climate model. *Int. J. Climatol.,* **31,** 1848–1865, doi:10.1002/joc.2201.

——, and Coauthors, 2010b: Technical description of version 4.0 of the Community Land Model. NCAR Tech. Note NCAR/TN-478+STR, 257 pp.

Qian, T., A. Dai, K. E. Trenberth, and K. W. Oleson, 2006: Simulation of global land surface conditions from 1948 to 2002: Part I: Forcing data and evaluations. *J. Hydrometeor.,* **7,** 953–975.

Qu, X., and A. Hall, 2007: What controls the strength of snow-albedo feedback? *J. Climate,* **20,** 3971–3981.

Ramankutty, N., A. T. Evan, C. Monfreda, and J. A. Foley, 2008: Farming the planet: 1. Geographic distribution of global agricultural lands in the year 2000. *Global Biogeochem. Cycles,* **22,** GB1003, doi:10.1029/2007GB002952.

Riley, W. J., Z. M. Subin, D. M. Lawrence, S. C. Swenson, M. S. Torn, L. Meng, N. Mahowald, and P. Hess, 2011: Barriers to predicting global terrestrial methane fluxes: Analyses using a methane biogeochemistry model integrated in CESM. *Biogeosciences,* **8,** 1925–1953, doi:10.5194/bg-8-1925-2011.

Sacks, W. J., B. I. Cook, N. Buenning, S. Levis, and J. H. Helkowski, 2009: Effects of global irrigation on the near-surface climate. *Climate Dyn.,* **33,** 159–175, doi:10.1007/s00382-008-0445-z.

Sakaguchi, K., and X. Zeng, 2009: Effects of soil wetness, plant litter, and under-canopy atmospheric stability on ground evaporation in the Community Land Model (CLM3. 5). *J. Geophys. Res.,* **114,** D01107, doi:10.1029/2008JD010834.

Stöckli, R., and Coauthors, 2008: The use of Fluxnet in the Community Land Model development. *J. Geophys. Res.,* **113,** doi:10.1029/2007JG000562.

Subin, Z. M., W. J. Riley, and D. Mironov, 2012: An improved lake model for climate simulations: Model structure, evaluation, and sensitivity analyses in, CESM1. *J. Adv. Model. Earth Syst.,* in press.

Tapley, B. D., S. Bettadpur, M. Watkins, and C. Reigber, 2004: The gravity recovery and climate experiment: Mission overview and early results. *Geophys. Res. Lett.,* **31,** L09607, doi:10.1029/2004GL019920.

Thornton, P. E., J.-F. Lamarque, N. A. Rosenbloom, and N. M. Mahowald, 2007: Influence of carbon–nitrogen cycle coupling on land model response to CO_2 fertilization and climate variability. *Global Biogeochem. Cycles,* **21,** GB4018, doi:10.1029/2006GB002868.

——, and Coauthors, 2009: Carbon–nitrogen interactions regulate climate-carbon cycle feedbacks: Results from an atmosphere-ocean general circulation model. *Biogeosciences,* **6,** 2099–2120.

Wang, A. H., and X. Zeng, 2009: Improving the treatment of the vertical snow burial fraction over short vegetation in the NCAR CLM3. *Adv. Atmos. Sci.,* **26,** 877–886.

Wang, X. J., and J. R. Key, 2005: Arctic surface, cloud, and radiation properties based on the AVHRR Polar Pathfinder dataset. Part I: Spatial and temporal characteristics. *J. Climate,* **18,** 2558–2574.

Xie, P. P., and P. A. Arkin, 1997: Global precipitation: A 17-year monthly analysis based on gauge observations, satellite estimates, and numerical model outputs. *Bull. Amer. Meteor. Soc.,* **78,** 2539–2558.

Zeng, X. B., and M. Decker, 2009: Improving the numerical solution of soil moisture-based Richards equation for land models with a deep or shallow water table. *J. Hydrometeor.,* **10,** 308–319.

Zeng, X. D., X. B. Zeng, and M. Barlage, 2008: Growing temperate shrubs over arid and semiarid regions in the Community Land Model–Dynamic Global Vegetation Model. *Global Biogeochem. Cycles,* **22,** GB3003, doi:10.1029/2007GB003014.

Zhang, T., J. A. Heginbottom, R. G. Barry, and J. Brown, 2000: Further statistics on the distribution of permafrost and ground ice in the Northern Hemisphere. *Polar Geogr.,* **24,** 126–131.